

By Huichan Zhao, Jonathan Jalving, Rukang Huang, Ross Knepper, Andy Ruina, and Robert Shepherd

A Helping Hand

Soft Orthosis with Integrated Optical Strain Sensors and EMG Control

Human fingers and hands are frequently injured because they are delicate, complex, and used constantly. More than 3 million people in the United States suffer from hand or forearm disabilities [1], and, worldwide, hand injuries account for one-third of all work injuries [2]. Due to the importance of hands and the prevalence of hand issues, there is an increasing effort toward developing hand orthotics. These efforts have resulted in active hand orthoses that have been used for rehabilitation training and restoring partial hand function [3]. To ensure safety and to reduce control complexity, some orthoses use mechanical

compliances [4], [5] such as underactuated linkages [6] or low-stiffness materials and structures (e.g., rubbers and flexible wires) [7], [8]–[11]. The orthoses made of elastomeric materials tend to be more comfortable, perhaps because their low elastic modulus ($10 \text{ kPa} < G' < 1 \text{ MPa}$) [12] is similar to that of human skin ($\sim 100 \text{ kPa}$) [13].

The orthotic systems made of elastomers, and powered with fluid pressure, show potential for both rehabilitation and gripping assistance [8]–[11]. For both purposes, the control must use sensory feedback (e.g., sensing of position, force, etc.) to apply the intended motions or forces. Commercially available flexible sensors usually suffer from low sensitivity, low repeatability, and signal drift. The liquid-metal-based resistive and soft-capacitive sensors can be sensitive, but they rely on expensive material or require a multistep construction

Digital Object Identifier 10.1109/MRA.2016.2582216
Date of publication: 18 August 2016

**Human fingers and hands
are frequently injured
because they are delicate,
complex, and used
persistently.**

process [14]–[16]. Computer vision can provide high-quality position sensing [17], but the camera systems, besides being costly and complex, can interfere with the user’s motion. Due to these sensor limitations, most soft orthotics do not use the camera systems; instead they are open loop.

To address these issues, we are developing a closed-loop-controlled soft orthotic with integrated curvature sensors. Our goal is to develop a low-cost soft orthotic that can be worn by a typical human hand and can provide enough tip force at each finger to be helpful for grasping light objects (e.g., fruits), while also providing finger position (defined as average curvature) control. We have achieved a reasonable functionality for these goals by using three advances described in this article: 1) a new rotational-casting technique, followed by an overmolding process for making the glove; 2) measuring finger motion through optical losses in a molded-into-place, etched,

plastic fiber-optic cable; and 3) controlling the motion with inexpensive, binary pneumatic switches controlled by a simple finite-state machine. The composite glove is purely polymeric, highly compliant, and provides little resistance to natural motion when it is not pressurized. When inflated, the fingers of the glove curve and stiffen.

Soft Orthotic Glove with Embedded Sensors and Actuators

Design

The glove has multiple functions: 1) it is an actively powered assistive device that helps each finger to bend independently; 2) it is a self-contained sensing device since the optical fibers that are molded into the fingers are curvature sensors, and, thus, they also approximately sense deflection even for passive motions with no actuation; and 3) by combining actuation and control, the glove is a robotic hand with fingers that can achieve the prescribed motions or forces (Figure 1).

The body of the glove is made of a silicone elastomer (ELASTOSIL M4601 A/B; Wacker Chemie AG), to which we added 10% Silicone Thinner from Smooth-On, Inc. Each finger has a series of interconnected air chambers and a relatively inextensible nylon fabric along the palm side of each finger (Figure 2), so, upon fluid pressurization, these actuators cause a grasping motion [18]. In the language of beam theory, the neutral axis for bending is just outside of this strain-limiting fabric and not in the middle of the finger. The finger mechanics are discussed further in the section “Actuator Motion Analysis.”

The optical-fiber sensors go from the root of the finger to the tip and back of it, bent in a “U” around the nylon fabric, and they are approximately in the bending beam’s neutral plane. At one end of each optical fiber is a light-emitting diode (LED). At the other end is a photodetector (a photodarlington that reacts to light intensity by amplifying a current). These transmitter–sensor pairs are held to the fiber ends with custom three-dimensional (3-D) printed holders, and they are powered via thin electrical wires (red and black, Figure 1). The pneumatic power comes from an external pressure source via tubes that are inserted into the

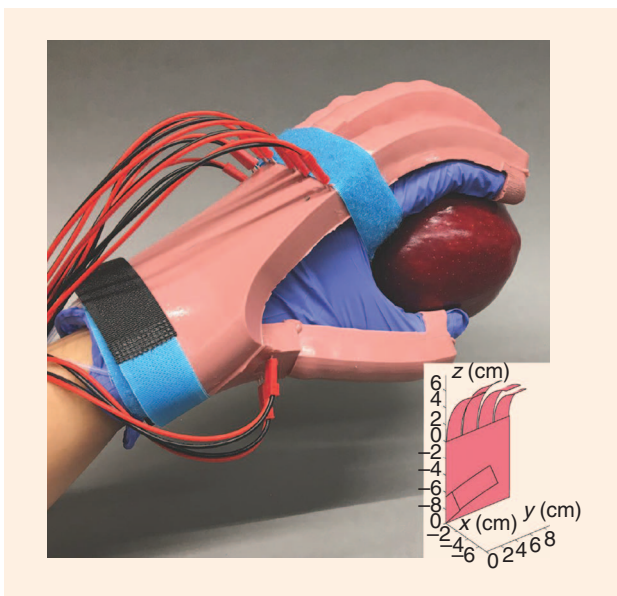


Figure 1. The glove is a soft orthosis. Here, it helps a limp human hand grasp an apple. The inset shows a computer representation of the finger shape, as estimated using the curvatures sensed by the embedded fiber-optic cables (these cables are the sensors used in the feedback control loop).

• **Due to the importance of hands and the prevalence of hand issues, there is an increasing effort toward developing hand orthotics.** •

holes molded into the wrist side of the glove. The tubes are connected to a pressure source via inexpensive three-position (pressurize, hold, and drain) electrical solenoid valves.

Actuator Motion Analysis

In this orthotic, each of the five fingers is made of a series of interconnected hollow spherical chambers. Figure 3(a) and (b) shows a single finger in two configurations: 1) its rest state, when the gauge pressure—the difference between the interior and exterior pressure—is zero, $\Delta p = 0$; and 2) bent to a curvature, $\kappa = 1/\rho$, caused by both the pressure difference, $\Delta p > 0$, and the bending load that the finger carries. To approximately calculate the curvature κ in terms of other parameters, we further simplify the finger model into a bending thin-wall cylindrical pressure vessel. The hoop strain (the increase in diameter of the cylindrical finger) is constrained by the struts (the walls between the spheres) [Figure 3(b)]. We model the strut structures by assuming the hoop strain is constrained [Figure 3(c)]. We model the whole cylindrical finger (the elastomer, stiff fabric at the bottom, gas pressure, and radial constraint) using a composite-beam model.

We presume the fabric at the finger bottom to be inextensible; thus, the beam-neutral axis is at the finger bottom. We assume that any external axial load is at the neutral axis so that it does not enter the bending calculations. For simplicity, we assume that the cylinder wall thickness t is much less than the finger radius r ($t \ll r$) and that the elastomer is linear and isotropic. The net moment M_N about the neutral axis is due to the axial elastic tension stress in the elastomer σ_{axial} (acting on the hollow cylinder with the radius r , thickness t , and moment of inertia about the neutral axis of $I_N = 3\pi r^3 t$), and that due to the gas pressure Δp (acting on the area πr^2 a distance r from the neutral axis)

$$M_N = - \int \sigma_{axial} y dA + r \cdot \Delta p \cdot (\pi r^2). \quad (1)$$

The equilibrium of the cylinder in the y direction [Figure 2(d)] gives a modified version of the standard thin-walled pressure-vessel formula

$$\Delta p \cdot r = \sigma_{hoop} t + T_s, \quad (2)$$

where σ_{hoop} is the hoop stress in the elastomer and T_s is a force per length that comes from the restraint against the hoop strain (against cylinder bulging). In the model here, the restraint represents the sidewall struts of the spheres. It could also represent restraint from the circumferential fibers [20] or from the interior foam [21]. As per conventional composite beam theory, we assume that the plane normal sections remain plane and normal, and, hence, the elastomer axial strain is given by

$$\epsilon_{axial} = \kappa y. \quad (3)$$

The linear elastic material properties of the elastomer are

$$\begin{aligned} \epsilon_{axial} &= \sigma_{axial}/E - \nu \sigma_{hoop}/E - \nu \sigma_{radial}/E, \\ \epsilon_{hoop} &= \sigma_{hoop}/E - \nu \sigma_{axial}/E - \nu \sigma_{radial}/E, \end{aligned} \quad (4)$$

where the elastomer elastic modulus is E and Poisson's ratio is ν .

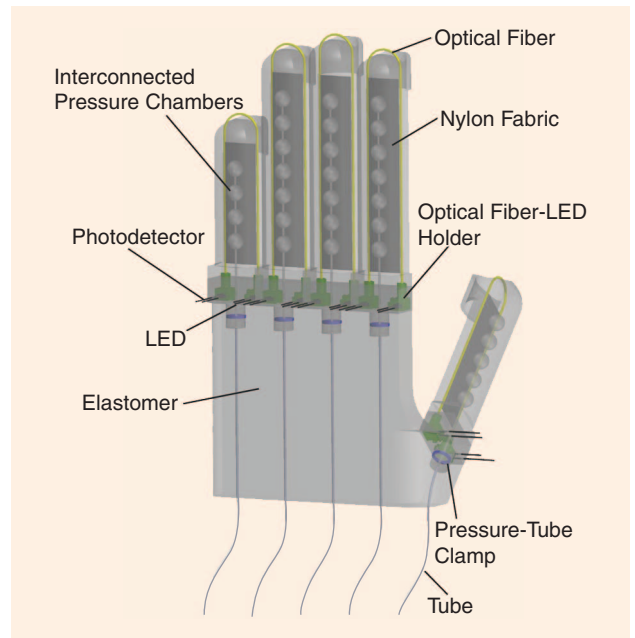


Figure 2. A schematic of the glove. Each component is labeled and exists on each finger: LEDs, pressure-chambers, optical fibers, photodetectors, nylon fabric, clamps, air-supply tubes, and optical-component holders.

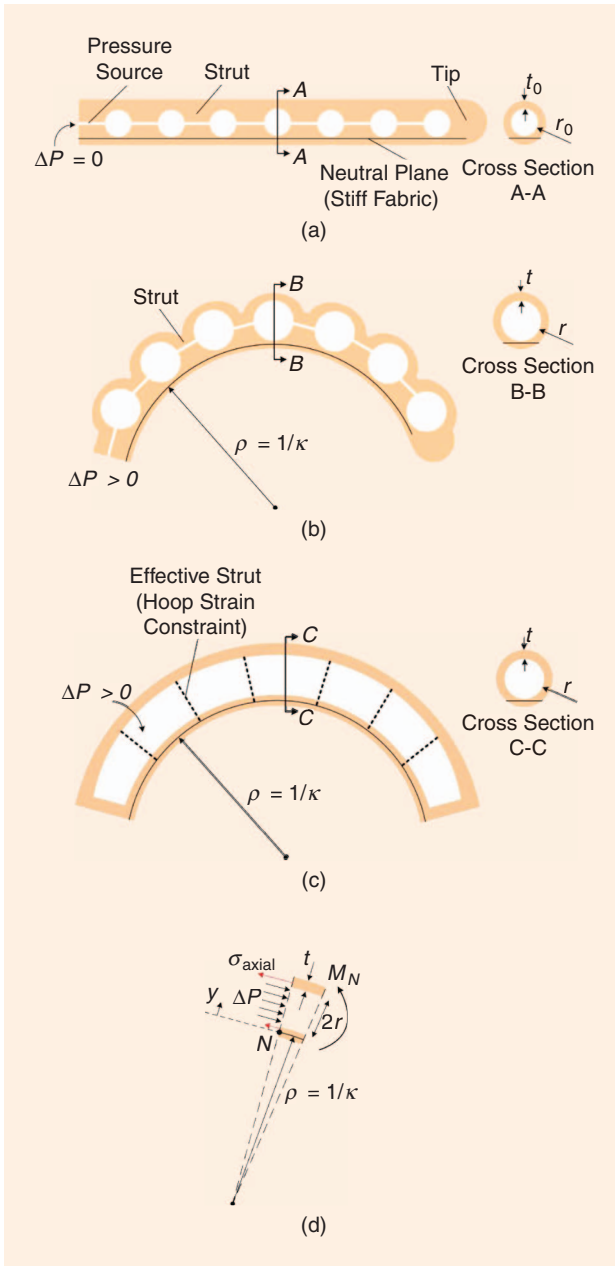


Figure 3. A schematic of one finger. (a) The rest state, with no loads and no pressure; (b) the bending equilibrium state, where the internal pressure is balanced by stretching the elastomer; (c) the simplified model of the bending equilibrium state: struts are replaced by a hoop strain constraint and other parameters stay the same; and (d) a free-body diagram of a short section of the finger actuator at the bending equilibrium state with both pressure and an externally induced moment M_N .

As per the standard pressure-vessel theory, in which the fluid pressure is much smaller than the vessel (elastomer) stresses, we neglect the radial stress, setting $\sigma_{\text{radial}} = 0$. As mentioned in regard to (2), we assume for simplicity that the restraint against bulging can be represented as a circumferential stress per unit length, T_s . Again, for simplicity, we think of these fibers as having modulus (force per unit length) E_f , so

$$T_s = E_f \epsilon_{\text{hoop}}. \quad (5)$$

With the substitution of (2)–(5) into (1) and integrating over the hollow cross section, we get

$$\kappa = -\frac{E_f - \nu^2 E_f + Et}{3\pi r^3 t (EE_f + E^2 t)} M_N + \frac{E_f - \nu^2 E_f - 2E\nu t + Et}{3t (EE_f + E^2 t)} \Delta p. \quad (6)$$

With no radial restraint ($E_f = 0$) and $\nu \sim 0.5$, which is the common approximation for elastomeric materials, the coefficient of Δp vanishes and the pressure has no effect on the curvature or bending moment. Thus, for the elastomeric fingers of this general design, the induction of curvature is entirely dependent on the restraint tension, T_s ; with no circumferential constraint, in this case from struts but possibly from interior foam or circumferential fibers, there is no bending due to pressure. The simplest approximation for this restraint is to assume that inextensible fibers, struts or what have you ($E_f = \infty$), in which case the relation between the pressure, curvature, and net finger moment is

$$\kappa = -\frac{1 - \nu^2}{3E\pi r^3 t} M_N + \frac{1 - \nu^2}{3Et} \Delta p. \quad (7)$$

This linear-elastic small-strain composite-beam model shows, for example, how the curvature increases with pressure and decreases with increasing elastomer modulus and elastomer thickness. Most importantly, the model shows the necessity of radial (circumferential) constraint in the elastomeric fingers for the pressure to cause bending, at least to the extent that this small-strain linear theory applies. When it is applied to long and narrow balloons ($\nu = 0.5$), the theory says that, to the first order, there is no elongation with pressurization. In reality, however, with large expansions, the long and narrow balloons do slightly elongate. Similarly, even without radial constraint, the elastomeric fingers will bend with large enough pressurization (violating the simple small strain theory here).

The maximum net finger moment can also be derived from (7) by setting $\kappa = 0$:

$$M_{N\text{max}} = \pi r^3 \Delta p. \quad (8)$$

When substituting $\Delta p = 270 \text{ kPa}$ and $r = 10 \text{ mm}$, we get $M_{N\text{max}} = 0.8 \cdot \text{N} \cdot \text{m}$. For an 8-cm-long finger, this yields a theoretical upper limit for the fingertip force of 10 N.

Manufacture of the Soft Orthotic Glove

Our orthotic glove is constructed by using a new rotational-casting technique followed by an overmolding process. The optical-fiber sensor is also fabricated from an innovative method.

Rotational Casting

There exist several methods to produce soft actuators [22], each with its own drawbacks. Replica molding (sometimes

referred to as *soft lithography*) can lead to delamination at the material bonds. Investment, or lost-wax, casting involves the building and destruction of molds for each part, which costs time and money. With the rotational casting, however, we have the molds that are reusable and that simultaneously produce multiple actuators that do not delaminate when pressurized (Figure 4) [19]. For this process, we 3-D print a mold, partially fill it with viscous pre-elastomers, fix the mold onto the

casting machine, and rotate it until the elastomer solidifies. Finally, we peel the actuators from the molds [Figure 4(c)].

Preparation of Optical-Fiber Sensors

Our strain sensor is a light-guide that is fabricated from one piece of a plastic optical fiber. First, using thermoforming at 50° C, we form the optical fiber into a U shape that allows us to reliably align it into the finger actuator (Figure 5). Then,

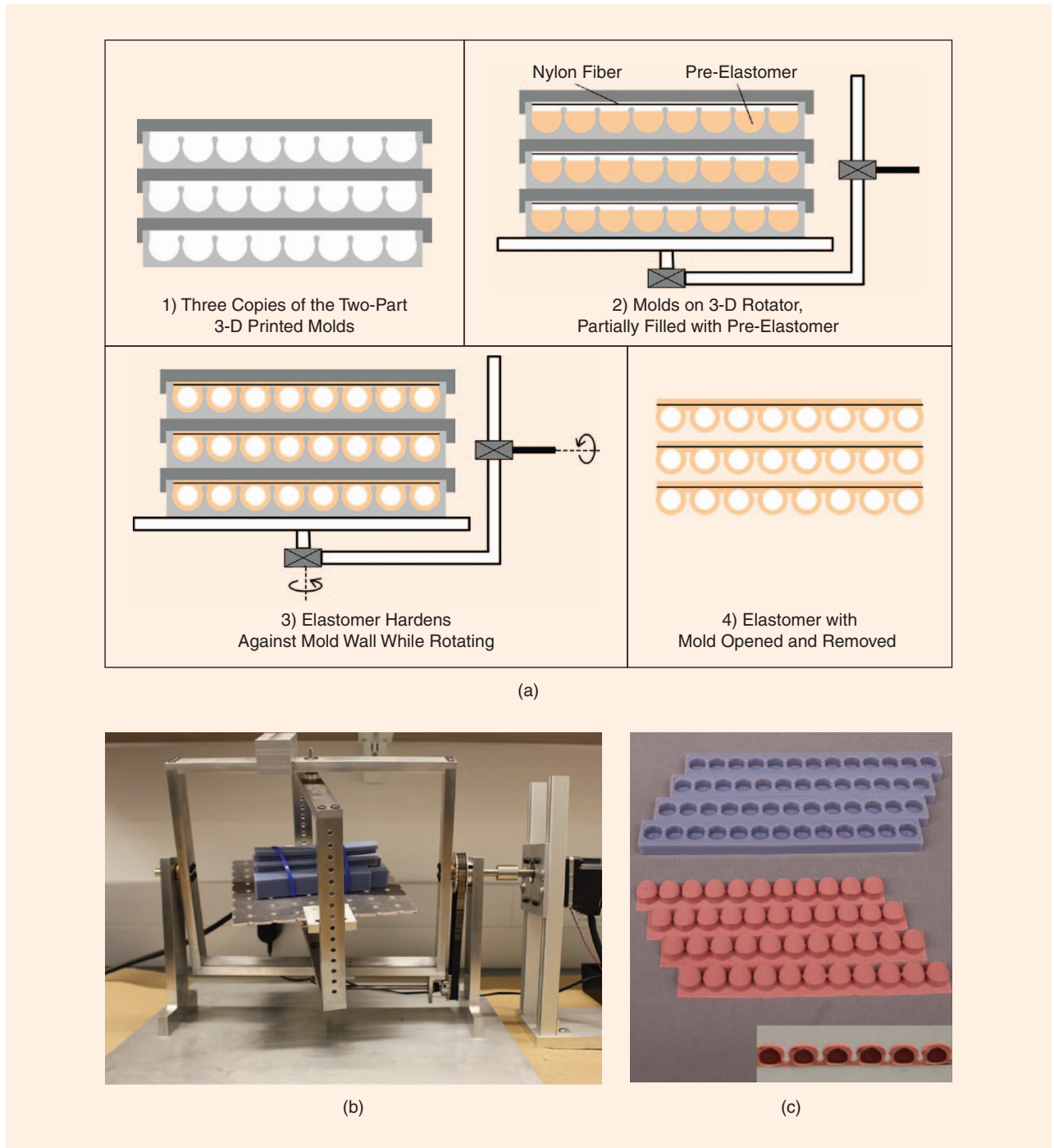


Figure 4. A rotational casting. (a) The casting process: 1) the molds, 2) the partially filled molds, 3) the rotational casting process, and 4) the final elastomer structure. (b) A rotational casting machine with multiple molds affixed. (c) The molds used (top) and the monolithic elastomers produced from those molds, with cross sections shown in the bottom right corner.

using a laser engraver (50 W Epilog Zing 24), we etch off a thin layer from one side of the U (lower right of Figure 5). Etching damages the cladding layer of the fiber, reducing the internal reflections, and part of the light is thus lost when traveling the length of the fiber. Because only one side is etched, the amount of light dissipation is affected by the bending; we measure this light amount change via a photodetector and correlate it to a curvature [23].

If too much of the fiber is engraved, the light dissipation can become saturated while the sensor is still in a working range of curvature. To ensure that our sensor lies below this saturation limit, we only engrave a sequence of short sections of the surface. The light-guide responds to both the extension and compression of the engraved side: the compression increases the signal intensity (preferable) and the extension decreases it. Therefore, we align the fibers within the fingers to operate in compression, which has an additional benefit of reducing the likelihood of fatigue fracture of the microcracks that we introduced during etching.

Overmolding

We assemble the rotational casting and the light-guide sensor in a 3-D printed finger mold, and we overmold them into a self-contained finger actuator. A steel wire is used to mold a connecting pathway between the internal actuators and is

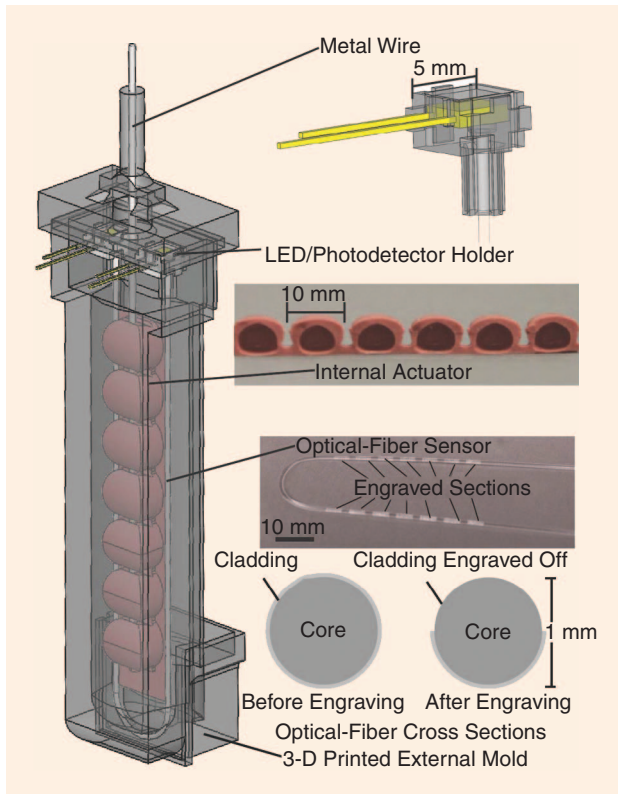


Figure 5. The overmolding of different components. Internal chambers of the actuator are aligned with the overmold. One end of the U-shaped light-guide attaches to the fixtures in the overmold. The fixtures are attached by the pins of the LED and a photodetector. After assembly, the silicone pre-elastomer is poured into the overmold to form a single finger actuator with sensors.

fixed in place using a 3-D printed mold cap (Figure 5). A custom 3-D printed fixture holds the LED, photodetector, and the optical-fiber sensor in the correct positions and orientations. After assembling, more silicone pre-elastomer is poured into the mold to overmold into a complete finger with the integral actuator and sensor. We cast five fingers of appropriate lengths into a complete hand orthotic.

Control System

The present control system uses a state machine controller, as shown in Figure 6. Each finger is controlled by its own

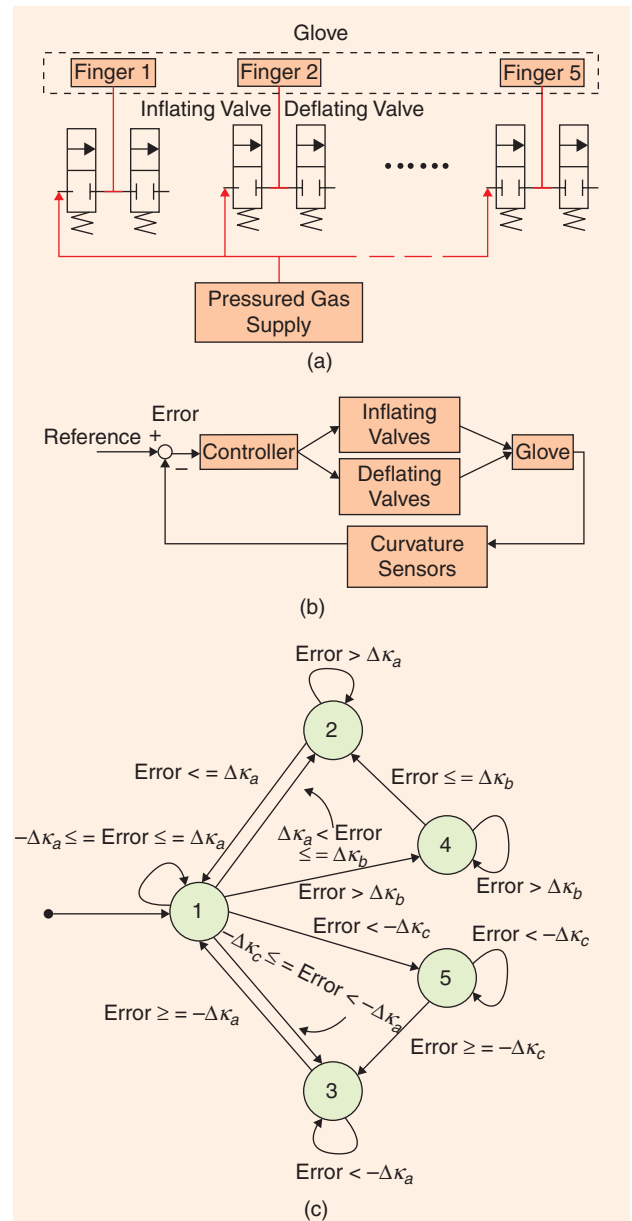


Figure 6. The control system: (a) a diagram showing how each finger is connected to the gas supply through valves; (b) a block diagram of the control system; and (c) a controller represented in a state machine diagram where the error is calculated from the current measured value subtracted from the targeted value, and $\Delta\kappa_a$, $\Delta\kappa_b$, and $\Delta\kappa_c$ are three threshold parameters to compare with the error; definitions of states 1–5 are in Table 1.

Table 1. Actions during states.

State	Inflating Valve	Deflating Valve	Comments
1	Off for Δt	Off for Δt	"Hold"
2	On for Δt , then Off for $X\Delta t$	Off for $(X + 1)\Delta t$	"In and hold"
3	Off for $(Y + 1)\Delta t$	On for Δt , then Off for $Y\Delta t$	"Out and hold"
4	On for Δt	Off for Δt	"In"
5	Off for Δt	On for Δt	"Out"

three-position valve (air in, hold, and air out), and each three-position valve is made from a pair of two-position valves (air in and air out) mounted to a pressure manifold. The simple nonlinear controller lets air into a finger to increase the curvature and lets air out to decrease curvature. If the curvature is close to the target (within a specified dead-band) then the flow is stopped, maintaining its gas volume and preventing set-point hunting. When approaching this dead-band region, the flow is stopped to prevent an overshoot.

The two-way valves are normally closed [Figure 6(a); X-valve, Parker Hannifin Corporation] and switched using power transistors (TIP120). The inflating valve connects the gas source to the actuator, and the deflating valve vents the actuator to the atmosphere. When the inflating valve is open and the deflating valve is closed, gas from the source pressurizes the actuator—the “in” state. When the inflating valve is closed and the deflating valve is open, gas vents from the actuator to the atmosphere—the “out” state. When both are closed, the gas remains inside the actuator—the “hold” state [Figure 6(a), (b)]. The viscoelasticity, gas compressibility, and gas-line resistance cause a lag between the valve decisions and sensed motion and leads to an overshoot. Creating a dead-band that is big enough to inhibit the resulting overshoot oscillations, however, leads to poor system accuracy. To prevent oscillations and maintain accuracy, we added state transitions to cut the flow or leakage before the acceptable target dead-band was sensed as reached [Figure 6(c) and Table 1]. This controller code is repeated ad infinitum at time intervals of $\Delta t = 5$ ms, as that is slightly longer than the timing required for the valves to open or close.

Each finger has its own state-machine controller, with each controller having five states. A state corresponds to a command to each three-position valve. The state transition conditions are based on the error $\Delta\kappa$ —the difference between the target and the measured curvatures. A check for a transition is made every controller cycle. There are three threshold parameters in the state-machine controller: an acceptably small error is specified as “ $\Delta\kappa_a$,” where a large-enough $\Delta\kappa_a$ prevents excessive attempts at correction, and $\Delta\kappa_b$ and $\Delta\kappa_c$ define the thresholds of the large-error region. When these thresholds are exceeded, inflation or deflation occurs, respectively. Between the high and low error regions, two settling time variables, X and Y , for positive and negative errors determine a remnant valve-off time. In effect, the valves are attenuated by $1/(X + 1)$

and $1/(Y + 1)$ in these intermediate-error bands. In general, $\Delta\kappa_a$ determines the accuracy of tracking but leads to an instability if set too small. Increasing $\Delta\kappa_b$ and $\Delta\kappa_c$ will increase stability but decrease the actuating speed. X and Y represents how long to wait during both the “in and hold” and “out and hold” states—increasing X and Y improves the stability and decreases speed. The valves are off in the dead-band, fully actuated toward the target when the error is large, and attenuated by $1/(X + 1)$ and $1/(Y + 1)$ in zones near the dead-band. In effect, this is an implementation of a three-level pulse-width modulation (PWM) system with three levels (all off, all on, and attenuated).

Experimental Results and Discussion

Calibration of Optical-Fiber Sensors

To calibrate the light-guides, we imaged each finger from the side while measuring the current output I from the photodetector (Figure 7). We calculated the curvature κ by picking four to seven points (determined by the number of chambers in the actuator) from each picture and fitting them to a circle. For curvature from 0 to 35 m^{-1} , the calibrations of all five fingers were linearly fit with a sensitivity ($\lambda \propto \Delta I/\Delta\kappa$) range of $0.23\text{ mA} \cdot \text{m} < \lambda < 0.49\text{ mA} \cdot \text{m}$. This sensitivity can be adjusted by changing both the engraving pattern and LED intensity. Other sensor features include: 1) a fast response time of 5 ms; 2) a high curvature resolution of 0.04 m^{-1} ; and 3) repeatability of 0.05 m^{-1} , measured by the standard deviation of a single curvature over five different tests. The response time, resolution, and repeatability outperform other sensing systems based on resistance and capacitance [14]–[16]. The sensor, however, has a nonlinear response beyond the range we tested; λ decreases at higher curvatures.

Force Test with the EMG Signal

We did a force test for each finger actuator [19] and the output tip force ranged from 0 to 5 N, by applying pressure ranging from 0 to 270 kPa [24]. This force output is similar to that of the fiber-reinforced soft actuators reported as hand assistive devices [9], [10], smaller than a cable-driven soft glove [7], and, at most, half of the theoretical upper-limit previously calculated. To better understand how this orthosis functions as a hand-assistive device, we measured the applied force of four fingers while monitoring the electromyography

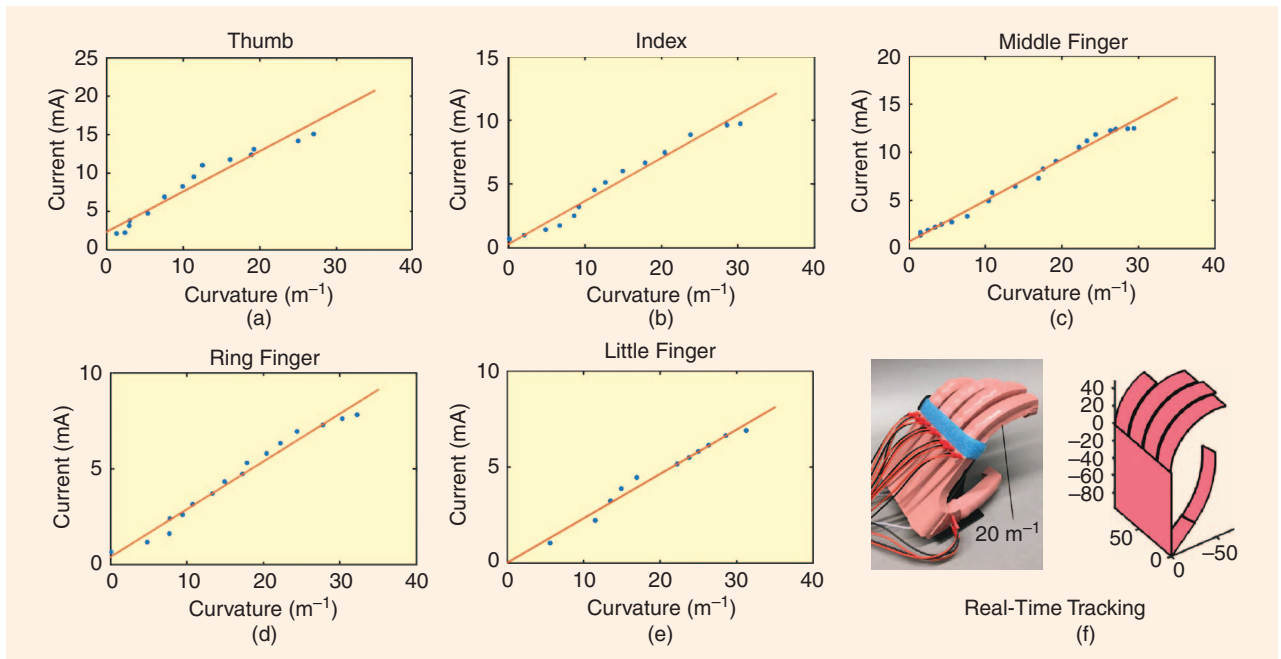


Figure 7. The light-guide calibration. A photodetector current output at various curvatures of the actuators. The blue dots are the measured results and the red lines are the linear fits. The last figure shows the real time curvature tracking of the glove after calibration where all fingers are bent at a curvature of 20 m^{-1} (5-cm radius).

(EMG) intensity as a measure of the user's effort [25]. A healthy user wore the glove and held a hand exerciser as shown in Figure 8. On each button of the hand exerciser, we attached a force sensor (FlexiForce A301 Sensor from Tekscan) to record the force exerted on it. Simultaneously, we measured the forearm muscle exertion using a Myo armband that uses eight EMG sensors that are applied uniformly around the forearm. The wearer pressed the four buttons to an average force of 1.0 N, and we then activated the orthosis. We observed an immediate increase in force from 1.0 N to 1.6 N, which then dropped to 1.4 N. We then depressurized the orthosis and observed an immediate drop in applied force to 0.3 N, which then rose up to 1.0 N. We repeated this process and received similar results. Finally, we asked the user to press the buttons to achieve a force of 1.6 N using solely their own effort.

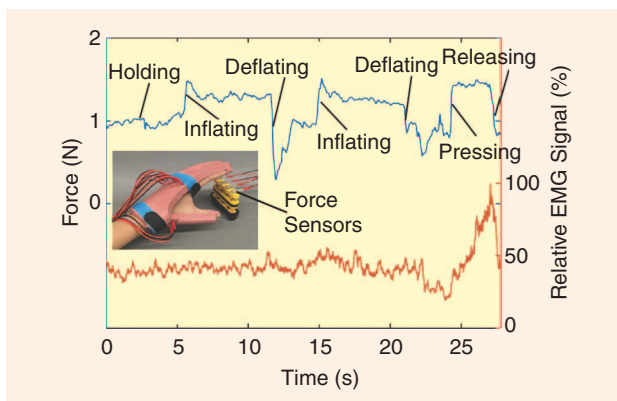


Figure 8. A force test with a worn glove. A hand exerciser with a force sensor attached to each button was held by the user, and the EMG signal was recorded at the same time.

From the aforementioned experiments, we saw that the actuator caused a significant and sudden overshoot force when activated and deactivated. The system then reached a stable state. During the later period, when the user was achieving 1.6 N of applied force from 1.0 N, we recorded an increase of the EMG intensity (the summation of all eight sensors of the armband). While the user was applying 1.0 N of force and the orthosis was augmenting to 1.6 N, the measured EMG intensity remained constant. This experiment demonstrated that the orthosis was assisting the user by augmenting his force by a factor of 1.6, saving muscular effort.

Control Results

To test our controller, we performed unloaded tracking tests for step changes in a curvature target. We ran the controller in an Arduino Mega microcontroller board, using the analogue and digital pins for sensor input and valve commands, respectively. We set $\Delta\kappa_a = 0.3 \text{ m}^{-1}$, $X = Y = 3$ (attenuation by 1/4 in near-dead-band zones) and chose three different values of $\Delta\kappa_b$ and $\Delta\kappa_c$.

We tested the controller's step response using various step stimuli for various durations (Figure 9). When $\Delta\kappa_b = \Delta\kappa_c = \Delta\kappa_a$, the controller is an on-off controller with a dead-band and no-transitional zone, leading to oscillations around the reference. When $\Delta\kappa_b = \Delta\kappa_c = 4\Delta\kappa_a$, we observed good accuracy (within 0.3 m^{-1} curvature), good stability (no oscillation or overshoot), and high speed (rise time of about 150 ms). When $\Delta\kappa_b = \Delta\kappa_c = 13\Delta\kappa_a$, a large intermediate attenuation zone, the rise time increased to 500 ms.

Many have explored the use of EMG signals for the control of orthotics [26]. We attempted to test whether

our orthotic had the potential to achieve this goal. We used a filtered EMG signal as a reference to represent a curvature target. While a Butterworth low-pass filter has been used with myoelectric signals [26], we found that a persistent force application by the fingers did not translate into a constant filtered signal. Instead, we collected an EMG signal from a user's forearm using the Myo armband at 200 Hz and used a moving average filter of 100 samples every 200 ms to produce a 5-Hz signal with less noise. We then fed this signal into our controller as the reference signal. Figure 10 shows both the raw EMG signal and the processed data for tracking. Our results show that the orthosis, using a state machine controller, can follow an EMG signal with a small overshoot and small oscillation.

Conclusions and Future Work

We designed both the hardware and a control method for a closed-loop soft orthosis. We performed the initial quantification of its force augmenting capabilities and the feedback control via optical-fiber sensors embedded into each actuator. We also showed that the orthotic can be used to track commands from an EMG signal. Our simplified linear mechanical analysis shows the key role of a radial, that is, circumferential, constraint for the functioning of the inflated elastomeric fingers. It also shows that stronger fingers are possible using circumferential unidirectional fibers around round-section polymeric fingers with the axial constraint at the finger bottom, which verifies prior experimental results [20].

Our system, promising as it is, however, needs improvement. First, our present choice of materials and actuator design do not yield enough force to conduct many common daily activities (e.g., opening a jar requires a torque of about 1–2 N·m [27], requiring tens of Newtons to grip a typical lid). Tougher materials, such as polyurethanes, along with a larger circumferential constraint, should allow us to achieve higher forces. Next, with a more refined state-machine controller, we should be able to improve the system's tracking ability. Finally, our sensing, and, hence, control, is limited to only the curvature. With compliant force sensors, we could achieve force or compliance control. Our hope is that the low cost of our device and controller will lead to devices that could be useful to a large population of patients who are in need of hand prostheses.

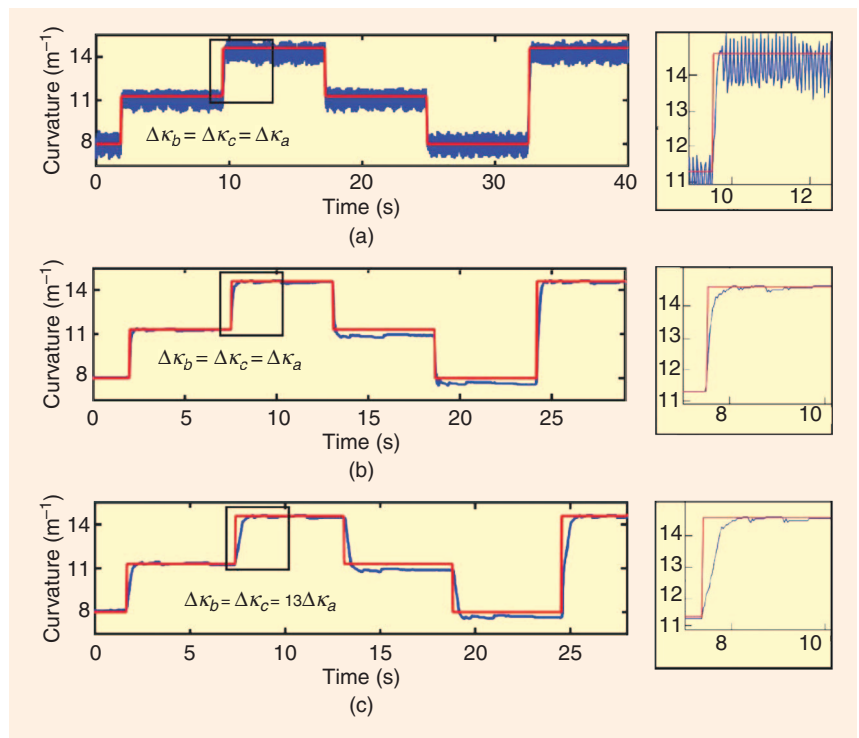


Figure 9. The step response of the controller with three different state-transition parameter sets. The red lines are the input signals and the blue lines are the measured system responses. The right plots show the enlarged views of the step-response data.

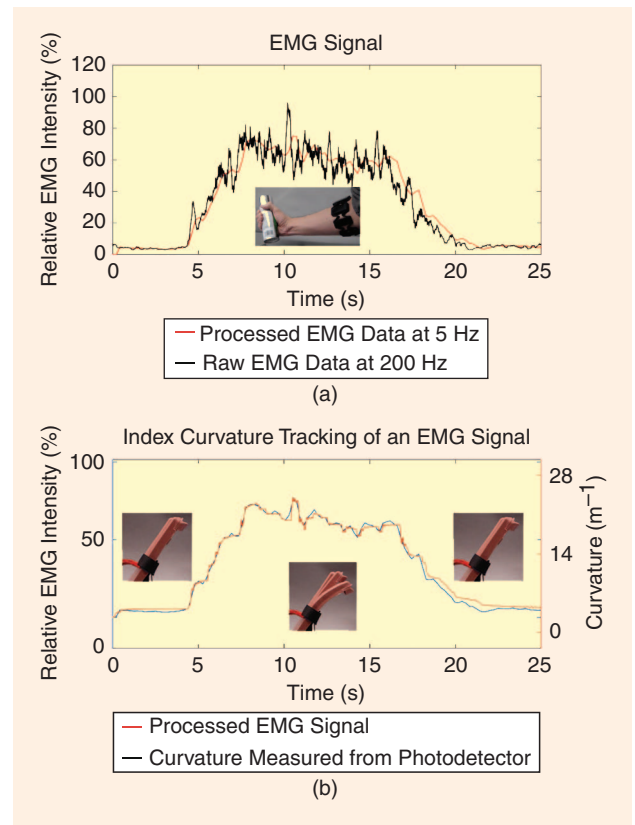


Figure 10. The index curvature tracking of an EMG signal previously collected from a healthy user.

References

- [1] R. C. Ficke. (1992, January). Digest of data on person with disabilities. *Department of Education. USA*. [Online]. Available: <http://eric.ed.gov/?id=ED347767>
- [2] J. Marty, B. Porcher, and R. Autissier, "Hand injuries and occupational accidents. Statistics and prevention," *Ann. Chir. Main*, vol. 2, no. 4, pp. 368–370, 1982.
- [3] P. Heo, G. M. Gu, S. Lee, K. Rhee, and J. Kim, "Current hand exoskeleton technologies for rehabilitation and assistive engineering," *Int. J. Precis. Eng. Man.*, vol. 13, no. 5, pp. 807–824, 2012.
- [4] Y. Hasegawa, Y. Mikami, K. Watanabe, and Y. Sankai, "Five-fingered assistive hand with mechanical compliance of human finger," in *Proc. IEEE Int. Conf. Robotics Automation*, Pasadena, CA, 2008, pp. 718–724.
- [5] A. Bicchi and G. Tonietti, "Fast and" soft-arm" tactics," *IEEE Robot. Automat. Mag.*, vol. 11, no. 2, pp. 22–33, 2004.
- [6] J. Iqbal, H. Khan, N. G. Tsagarakis, and D. G. Caldwell, "A novel exoskeleton robotic system for hand rehabilitation—Conceptualization to prototyping," *Biocybern. Biomed. Eng.*, vol. 34, no. 2, pp. 79–89, 2014.
- [7] H. In, B. B. Kang, M. Sin, and K. Cho, "Exo-Glove: A Wearable Robot for the Hand with a Soft Tendon Routing System," *IEEE Robot. Automat. Mag.*, vol. 22, no. 1, pp. 97–105, 2015.
- [8] P. Polygerinos, K. C. Galloway, E. Savage, M. Herman, K. O. Donnell, and C. J. Walsh, "Soft robotic glove for hand rehabilitation and task specific training," in *Proc. IEEE Int. Conf. Robotics Automation*, Seattle, WA, 2015, pp. 2913–2919.
- [9] H. K. Yap, J. H. Lim, F. Nasrallah, F. Z. Low, J. C. Goh, and R. C. Yeow, "MRC-glove: A fMRI compatible soft robotic glove for hand rehabilitation application," in *Proc. IEEE ICORR*, Singapore, 2015, pp. 735–740.
- [10] P. Polygerinos, K. C. Galloway, S. Sanan, M. Herman, and C. J. Walsh, "EMG controlled soft robotic glove for assistance during activities of daily living," in *Proc. IEEE ICORR*, Singapore, 2015, pp. 55–60.
- [11] J. H. Low, M. H. Ang, and C. H. Yeow, "Customizable soft pneumatic finger actuators for hand orthotic and prosthetic applications," in *Proc. IEEE ICORR*, Singapore, 2015, pp. 380–385.
- [12] D. Rus and M. T. Tolley, "Design, fabrication and control of soft robots," *Nature*, vol. 521, no. 7553, pp. 467–475, 2015.
- [13] P. G. Agache, C. Monneur, J. L. Leveque, and J. De Riga, "Mechanical properties and Young's modulus of human skin in vivo," *Arch. Dermatol. Res.*, vol. 269, no. 3, pp. 221–232, 1980.
- [14] R. L. Hammond, Y. Menguc, and R. J. Wood, "Toward a modular soft sensor-embedded glove for human hand motion and tactile pressure measurement," in *Proc. IEEE/RSJ Int. Conf. Intelligent Robots Systems*, Chicago, IL, 2014, pp. 4000–4007.
- [15] J. Chossat, Y. Tao, V. Duchaine, and Y. Park, "Wearable soft artificial skin for hand motion detection with embedded microfluidic strain sensing," in *Proc. IEEE Int. Conf. Robotics Automation*, Seattle, WA, 2015, pp. 2568–2573.
- [16] P. Roberts, D. D. Damian, W. Shan, T. Lu, and C. Majidi, "Soft-matter capacitive sensor for measuring shear and pressure deformation," in *Proc. IEEE Int. Conf. Robotics Automation*, Karlsruhe, Germany, 2013, pp. 3529–3534.
- [17] A. D. Marchese, K. Komorowski, C. D. Onal, and D. Rus, "Design and control of a soft and continuously deformable 2-D robotic manipulation system," in *Proc. IEEE Int. Conf. Robotics Automation*, Hong Kong, China, 2014, pp. 2189–2196.
- [18] R. F. Shepherd, F. Ilievski, W. Choi, S. A. Morin, A. A. Stokes, A. D. Mazzeo, X. Chen, M. Wang, and G. M. Whitesides, "Multigait soft robot," *Proc. Nat. Acad. Sci. U.S.A.*, vol. 108, no. 51, pp. 20400–20403, 2011.
- [19] H. Zhao, Y. Li, A. Elsamadisi, and R. F. Shepherd, "Scalable manufacturing of high force wearable soft actuators," *Extreme Mech. Lett.*, vol. 3, pp. 89–104, 2015.
- [20] R. Deimel and Oliver Brock, "A compliant hand based on a novel pneumatic actuator," in *Proc. IEEE Int. Conf. Robotics Automation*, Karlsruhe, Germany, 2013, pp. 2047–2053.
- [21] B. C. Mac Murray, X. An, S. S. Robinson, I. M. van Meerbeek, K. W. O'Brien, H. Zhao, and R. F. Shepherd, "Poroelastic foams for simple fabrication of complex soft robots," *Adv. Mater.*, vol. 27, no. 41, pp. 6334–6340, 2015.
- [22] A. D. Marchese, R. K. Katzschmann, and D. Rus, "A recipe for soft fluidic elastomer robots," *Soft Robotics*, vol. 2, no. 1, pp. 7–25, 2015.
- [23] A. Djordjevic and M. Boskovic, "Curvature gauge," *Sensor. Actuat. A Phys.*, vol. 51, no. 2, pp. 193–198, 2002.
- [24] H. Zhao, R. Huang, and R. F. Shepherd, "Curvature control of soft orthotics via low cost solid-state optics," in *Proc. IEEE Int. Conf. Robotics Automation*, Stockholm, Sweden, 2016, pp. 4008–4013.
- [25] O. M. Blake and J. M. Wakeling, "Estimating changes in metabolic power from EMG," *SpringerPlus*, vol. 2, no. 1, pp. 1–7, 2013.
- [26] M. DiCicco, L. Lucas, and Y. Matsuoka, "Comparison of control strategies for an EMG controlled orthotic exoskeleton for the hand," in *Proc. IEEE Int. Conf. Robotics Automation*, New Orleans, LA, 2004, pp. 1622–1627.
- [27] A. I. M. Voorbij and L. P. A. Steenbekkers, "The twisting force of aged consumers when opening a jar," *Appl. Ergon.*, vol. 33, no. 1, pp. 105–109, 2002.

Huichan Zhao, Sibley School of Mechanical and Aerospace Engineering, Cornell University, Ithaca, New York. E-mail: h2282@cornell.edu.

Jonathan Jalving, Sibley School of Mechanical and Aerospace Engineering, Cornell University, Ithaca, New York. E-mail: jej93@cornell.edu.

Rukang Huang, Sibley School of Mechanical and Aerospace Engineering, Cornell University, Ithaca, New York. E-mail: rh457@cornell.edu.

Ross Knepper, Department of Computer Science, Cornell University, Ithaca, New York. E-mail: rak@cs.cornell.edu.

Andy Ruina, Sibley School of Mechanical and Aerospace Engineering, Cornell University, Ithaca, New York. E-mail: ruina@cornell.edu.

Robert Shepherd, Sibley School of Mechanical and Aerospace Engineering, Cornell University, Ithaca, New York. E-mail: rfs247@cornell.edu.

